Probabilistic Road Geometry Estimation using a Millimetre-Wave Radar

Andres Hernandez-Gutierrez, Juan I. Nieto, Tim Bailey and Eduardo M. Nebot

***Abstract*— This paper presents a probabilistic framework for road geometry estimation using a millimetre wave radar. It aims at estimating the geometry of unpaved and unmarked roads, and also provides the vehicle location with respect to the edges of the road. This road tracking system employs a radar sensor due to its robustness to weather conditions such as fog, dust, rain and snow. The proposed approach is robust to noisy measurements because the radar target locations are modelled as Gaussian distributions. These observations are integrated into a Kalman Particle filter to estimate the *posterior* distribution of the parameters that best describe the geometry of the road. Experimental results using data acquired on a highway road are presented. The effectiveness of the proposed approach is demonstrated by a qualitative analysis of the results.**

I. INTRODUCTION

Road detection and tracking refers to the process of locating the road surface and its boundaries. Depending on the type of road and environment, this process can be accomplished by gathering information from sensors such as video cameras, laser rangefinders, GPS receivers together with digital maps, and more recently using radar sensors. Road tracking systems are of significant importance in both autonomous systems and in advance driving assistance systems. In these applications, the automobile has to localise itself with respect to the edges of the road in order to perform its next task. The first lane recognition system dates back 25 years when a vision-based approach using the Kalman filter was proposed in [1]. Subsequent versions of this work, which analysed spatio-temporal information and extended the curve estimation to 3D space, were presented in [2] and [3]. These implementations were then followed by the ARCADE algorithm (*Automated Road Curvature And Direction Estimation*) in [4]. It estimates the curvature and orientation of the road based on features extracted from monochromatic images in combination with a model of the road, providing appropriate results for marked roads. A vision-based system for lane recognition, using a particle filter approach, was developed in [5]. A method based on multiple features such as edges, texture and colour extracted from images was presented in [7].

Although the first implementations for road detection were vision-based systems, the detection and tracking of roads has also been attempted by the employment of laser rangefinders. Implementations of these systems are proposed in [8] and [9]. Techniques that fuse information from multiple sensors are given in [10] and [11], and more recently in [12]. All these implementations provide reliable results in moderate weather conditions; nevertheless, their main disadvantages are the lack of robustness against environmental conditions such as dust, fog, snow and rain in which their performance could be degraded. Therefore, it is necessary to utilise a sensor that is capable of providing reliable information even if adverse environmental factors are present.

Radar sensors are less susceptible to these environmental conditions [13], [14]; hence, automobile manufactures have recently equipped vehicles with radar sensors to perform tasks such as collision avoidance, traffic scene interpretation and dynamic object detection. Unlike a laser rangefinder, which emits a coherent light beam, a radar sensor radiates a wide directive beam that illuminates part of a surface. In general, a measurement at a given bearing angle consists of various returns from targets detected in the radar footprint area; however, due to the sidelobes found in the radiation pattern, highly reflective objects located near the radar footprint area could generate an erroneous range measurement at that bearing angle. This is because all measurements are assumed to be detected at the centre line of the radar beam. Another concern when using a radar sensor refers to clutter signals. In a road tracking system, these signals correspond to targets located far from the edges of the road, radar returns corresponding to dynamic objects or multipath echoes due to multiple reflections. Therefore, a challenging task when using a radar sensor is being able to surmount this extra complexity while taking advantage of its immunity to most of the weather conditions.

The work presented in this paper aims at developing a probabilistic approach for detection and tracking of both unpaved and unmarked roads, with robustness to normal and harsh environmental conditions such as those found in mining roads. The *posterior* probability density function (pdf) of the parameters that best describe the geometry of the road and the vehicle location with respect to the edges of the road are the output of a Kalman particle filter.

This paper is organised as follows. An overview of the proposed algorithm is given in section II. A description of the model used to represent the road is detailed in section III. Section IV explains how the radar observations are modelled as Gaussian distributions, which are subsequently used in section V to estimate the road geometry parameters. Experimental results in section VI are followed by the conclusions in section VII.

Andres Hernandez-Gutierrez, Juan I. Nieto, Tim Bailey and Eduardo M. Nebot are with the Australian Centre for Field Robotics. School of Aerospace, Mechanical and Mechatronic Engineering. The University of Sydney NSW 2006, Australia. {a.hernandez, j.nieto, t.bailey, nebot}@acfr.usyd.edu.au

II. ALGORITHM OVERVIEW

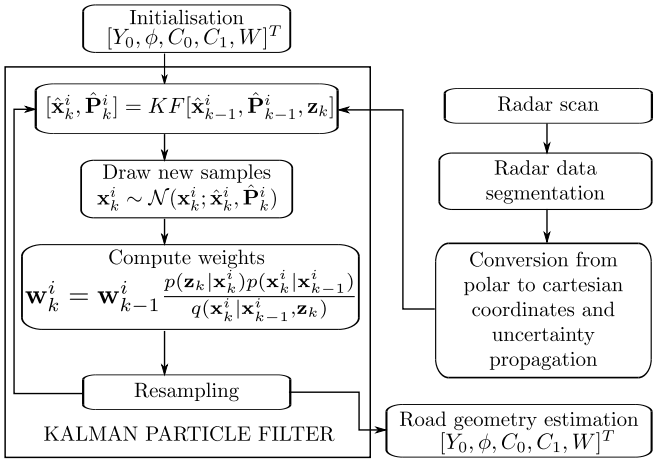

Fig. 1. Block diagram of the road geometry estimation process.

Fig. 1 shows a block diagram of the probabilistic road tracking system proposed in this work. It estimates the relative vehicle location, Y_0, with respect to the left edge of the road as well as other road geometry parameters, such as the orientation angle of the road, ϕ, with respect to the radar coordinate frame, the curvature, C_0, the rate of curvature, C_1, and the width of the road, W.

A radar measurement comprises a 180-degree scan that may contain radar information belonging to objects detected on the road, edges of the road or reflective targets located near the borders. This information is first segmented in order to extract useful radar data corresponding to the boundaries. By analysing the intensity level of the radar returns and signal noise along the complete trajectory, it has been observed that valuable information can be extracted by thresholding, setting the threshold value at $65dB$. Subsequently, a conversion from polar to Cartesian coordinates is applied to this data. This stage is followed by the uncertainty propagation from polar to Cartesian coordinates, which takes into account the uncertainty in range and bearing of the radar sensor.

The road edges are modelled as a pair of clothoid curves parametrised by the elements of $\mathbf{x} = [Y_0,\ \phi,\ C_0,\ C1,\ W]^T$. A Kalman particle filter is used to estimate these parameters by generating N hypotheses at each time step k. First, for each hypotesis $\hat{\mathbf{x}}_{k-1}^i$, $i = 1,\ldots,N$, the Mahalanobis distance is used to associate the radar observations, $\mathbf{z}_k$, to the left or right clothoid curve, then after the prediction stage in the Kalman filter, each hypothesis is updated and its mean, $\hat{\mathbf{x}}_k^i$, and covariance matrix, $\hat{\mathbf{P}}_k^i$, are used to build a proposal distribution. This proposal distribution is used to sample new particles. Subsequently, using the transitional density function, the sensor likelihood function and the proposal distribution, the weight for every hypothesis is obtained. Particles having the highest weights are selected in the resampling stage and are used to represent the geometry of the road.

III. CLOTHOID CURVE FOR ROAD GEOMETRY ESTIMATION

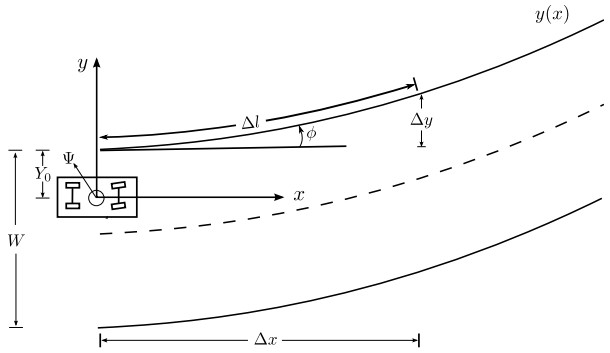

Fig. 2. Road model represented by a cubic approximation of a Clothoid function.

Clothoid curves have been used in civil engineering [15] for road design in order to geometrically join a straight road to a curve road. The main characteristic of a Clothoid function is that its curvature is proportional to the length of the curve measured from its origin [1].

$$C(l) = C_0 + C_1 * l \tag{1}$$

where C_0 and $C_1 = \frac{dC}{dl}$ are the curvature and rate of curvature of the road respectively. Fig. 2 shows a plane curve that is parametrised by the first integral of curvature given by the heading direction $\phi(l)$, and the second integrals represented by $x(l)$ and $y(l)$ listed below. Substituting l by τ for integration purposes, it yields

$$\phi(l) = \phi_0 + \int_0^l C(\tau)\ d\tau \tag{2}$$

$$x(l) = x_0 + \int_0^l cos\ \phi(\tau) d\tau \tag{3}$$

$$y(l) = y_0 + \int_0^l sin\ \phi(\tau) d\tau \tag{4}$$

substituting (1) in (2) and solving in terms of τ yields

$$\phi(\tau) = \phi_0(\tau) + C_0\tau + \frac{1}{2}C_1\tau^2 \tag{5}$$

If $\phi(\tau)$ is substituted in (3) and (4), it would require to solve Fresnel's Integrals. Instead, provided the vehicle heading changes are less than 10^o, that is, $|\phi| < 10^o$, the approximation of $\cos\phi \approx 1$ and $\sin\phi \approx \phi$ remains valid. Assuming this constraint, and solving (3), the parametric function $x(l)$ can be rewritten as

$$x(l) = x_0(l) + l \tag{6}$$

setting $x_0(l) = 0$ leads to $x(l) = l$, and the parametric function $y(l)$ is then given by

$$y(l) \approx Y_0 + \phi l + \frac{1}{2}C_0 l^2 + \frac{1}{6}C_1 l^3 \tag{7}$$

The road model used to represent the left curve in terms of the longitudinal distance x is obtained by substituting $x(l) = l$ in (7) which yields

$$y(x) \approx Y_0 + \phi x + \frac{1}{2}C_0 x^2 + \frac{1}{6}C_1 x^3 \tag{8}$$

We assume that both the left and right curve are parallel; therefore, the left curve is offset to the right by the width of the road in order to obtain the Clothoid curve that represents the right boundary. The state vector $\mathbf{x}$ to be estimated by the Kalman particle filter is given by

$$\mathbf{x} = \begin{bmatrix} Y_0 & \phi & C_0 & C_1 & W \end{bmatrix}^T \tag{9}$$

where these parameters represent the lateral offset with respect to the left border, the orientation of the road with respect to the vehicle coordinate frame, the curvature, rate of curvature, and the width of the road respectively.

IV. PREPROCESSING RADAR INFORMATION

A single radar return is $\hat{\mathbf{a}} = (r, \theta)$, where r is range and θ is bearing, and is modelled as $\mathbf{a} \sim \mathcal{N}(\hat{\mathbf{a}}, \mathbf{P_a})$, with mean $\hat{\mathbf{a}}$ and covariance matrix $\mathbf{P_a}$. For the road estimation process, every radar observation is converted from polar to Cartesian coordinates using the nonlinear transformation $\mathbf{g}(\cdot)$.

$$\hat{\mathbf{z}} = \begin{bmatrix} \hat{x} \\ \hat{y} \end{bmatrix} = \mathbf{g}(\mathbf{a}) = \begin{bmatrix} r \cdot cos\ \theta \\ r \cdot sin\ \theta \end{bmatrix} \tag{10}$$

The covariance matrix associated with every radar return in polar coordinates is

$$\mathbf{P} = \begin{bmatrix} \sigma_r^2 & 0 \\ 0 & \sigma_\theta^2 \end{bmatrix} \tag{11}$$

where σ_r and σ_θ is the standard deviation of the uncertainty in range and bearing. Through a linearisation approach, the density of $\mathbf{z}$ is modelled by a Gaussian distribution with mean $\hat{\mathbf{z}}$ and covariance matrix $\mathbf{R}$.

$$\mathbf{R} = \nabla\mathbf{g}(\mathbf{z})\ \mathbf{P}\ \nabla\mathbf{g}^T(\mathbf{z}) \tag{12}$$

where $\mathbf{g}(\mathbf{z})$ is the Jacobian of $\mathbf{g}(\cdot)$ given by

$$\nabla\mathbf{g}(\mathbf{z}) = \frac{\partial\mathbf{g}(\mathbf{z})}{\partial\mathbf{a}} = \begin{bmatrix} cos\ \theta & sin\ \theta \\ -r \cdot sin\ \theta & r \cdot cos\ \theta \end{bmatrix} \tag{13}$$

V. ROAD EXTRACTION USING RADAR DATA

The Kalman particle filter is a recursive Bayesian estimator based on Monte Carlo sampling methods [16]. Particle filter based estimation methods have the advantage of not being subject to any linearity or Gaussianity constraint on both the prediction and observation models [5]. In the *Sequential Importance Resampling* filter *SIR*, the posterior probability distribution is represented by weights $\mathbf{w}_k^i$ associated to a set of particles $\mathbf{x}_k^i$. The importance weights up to a normalising constant are evaluated as

$$\tilde{\mathbf{w}}_k^i = \mathbf{w}_{k-1}^i\ \frac{p(\mathbf{z}_k|\mathbf{x}_k^i)p(\mathbf{x}_k^i|\mathbf{x}_{k-1}^i)}{q(\mathbf{x}_k^i|\mathbf{x}_{k-1}^i, \mathbf{z}_k)} \tag{14}$$

A common proposal distribution is given by the prediction model $p(\mathbf{x}_k^i|\mathbf{x}_{k-1}^i)$, which gives importance weights as (15). However, this proposal distribution does not explore the sample space efficiently. It has been demonstrated in [17] that the importance density distribution that minimises the variance of the importance weights, provided $\mathbf{x}_{k-1}^i$ and $\mathbf{z}_k$, is given by (16).

$$\tilde{\mathbf{w}}_k^i = \mathbf{w}_{k-1}^i\ p(\mathbf{z}_k|\mathbf{x}_k^i) \tag{15}$$

$$q(\mathbf{x}_k^i|\mathbf{x}_{k-1}^i, \mathbf{z}_k) = \frac{p(\mathbf{z}_k|\mathbf{x}_k^i, \mathbf{x}_{k-1}^i)p(\mathbf{x}_k^i|\mathbf{x}_{k-1}^i)}{p(\mathbf{z}_k|\mathbf{x}_{k-1}^i)} \tag{16}$$

substituting (16) back into (14) yields:

$$\tilde{\mathbf{w}}_k^i = \mathbf{w}_{k-1}^i\ \frac{p(\mathbf{z}_k|\mathbf{x}_{k-1}^i)p(\mathbf{z}_k|\mathbf{x}_k^i)p(\mathbf{x}_k^i|\mathbf{x}_{k-1}^i)}{p(\mathbf{z}_k|\mathbf{x}_k^i, \mathbf{x}_{k-1}^i)p(\mathbf{x}_k^i|\mathbf{x}_{k-1}^i)} \tag{17}$$

$$\tilde{\mathbf{w}}_k^i = \mathbf{w}_{k-1}^i\ \frac{p(\mathbf{z}_k|\mathbf{x}_{k-1}^i)p(\mathbf{z}_k|\mathbf{x}_k^i)}{p(\mathbf{z}_k|\mathbf{x}_k^i, \mathbf{x}_{k-1}^i)} \tag{18}$$

because $\mathbf{z}_k$ is conditional independent of $\mathbf{x}_{k-1}^i$, we obtain

$$\tilde{\mathbf{w}}_k^i = \mathbf{w}_{k-1}^i\ \frac{p(\mathbf{z}_k|\mathbf{x}_{k-1}^i)p(\mathbf{z}_k|\mathbf{x}_k^i)}{p(\mathbf{z}_k|\mathbf{x}_k^i)} \tag{19}$$

$$\tilde{\mathbf{w}}_k^i = \mathbf{w}_{k-1}^i\ p(\mathbf{z}_k|\mathbf{x}_{k-1}^i) \tag{20}$$

which expresses that importance weights at time k can be computed before the particles are propagated to time k. This is an important aspect when the vehicle is approaching a road that has a small radius of curvature. In contrast, when using (15), the weights are computed using the propagated particles that were based on the previous estimation. Hence if the road has a small radius of curvature, the propagated particles (Clothoid curves) could probably diverge from where the actual radar observations are being detected. As a result, the filter would not provide an appropriate estimation of the paramaters.

An option to estimate the optimal proposal distribution in (16) is applying the Kalman filter which encourages the particles to move into a region of high likelihood. That is, it corrects the particles and compute the covariance matrix for each hypothesis and a new particle is sampled from a Gaussian proposal distribution with mean and covariance given by the updated parameters in the Kalman filter. Although the computational cost when applying the KF to each particle increases, it is compensated by a reduction of the number of samples required to achieve a certain level of performance since the particles have been corrected. For this reason, we have adopted the Kalman Particle filter approach in this work.

The pseudo-code of the Kalman particle filter implemented here is listed in Algorithm 1. The resampling approach used in this algorithm is the stratified sampling. The number of particles N was set to 1000.

Algorithm 1 Kalman Particle Filter

$[\{\mathbf{x}_k^j, \mathbf{w}_k^j, \mathbf{P}_k^j\}_{j=1}^N] = \text{KPF}[\{\mathbf{x}_{k-1}^i, \mathbf{w}_k^i, \mathbf{P}_{k-1}^i\}_{i=1}^N, \mathbf{z}_k]$
for $i = 1$ **to** N **do**
  $[\hat{\mathbf{x}}_k^i, \hat{\mathbf{P}}_k^i] = \text{KF}[\mathbf{x}_{k-1}^i, \mathbf{P}_{k-1}^i, \mathbf{z}_k]$
  $\mathbf{x}_k^i \sim \mathcal{N}(\mathbf{x}_k^i; \hat{\mathbf{x}}_k^i, \hat{\mathbf{P}}_k^i)$
  $\tilde{\mathbf{w}}_k^i = \mathbf{w}_{k-1}^i \frac{p(\mathbf{z}_k|\mathbf{x}_k^i)\ p(\mathbf{x}_k^i|\mathbf{x}_{k-1}^i)}{q(\mathbf{x}_k^i|\mathbf{x}_{k-1}^i, \mathbf{z}_k)}$
  where $q(\mathbf{x}_k^i|\mathbf{x}_{k-1}^i, \mathbf{z}_k) = \mathcal{N}(\mathbf{x}_k^i; \hat{\mathbf{x}}_k^i, \hat{\mathbf{P}}_k^i)$
end for
$t = SUM[\{\tilde{\mathbf{w}}_k^i\}_{i=1}^N]$
for $i = 1$ **to** N **do**
  $\mathbf{w}_k^i = t^{-1}\tilde{\mathbf{w}}_k^i$
end for
$\tilde{N}_{eff} = \frac{1}{\sum_{i=1}^N (\mathbf{w}_k^i)^2}$
if $\tilde{N}_{eff} < \frac{N}{2}$ **then**
  $[\{\mathbf{x}_k^i, \mathbf{w}_k^i\}_{i=1}^N] = \text{RESAMPLE}[\{\mathbf{x}_k^i, \mathbf{w}_k^i\}_{i=1}^N]$
end if

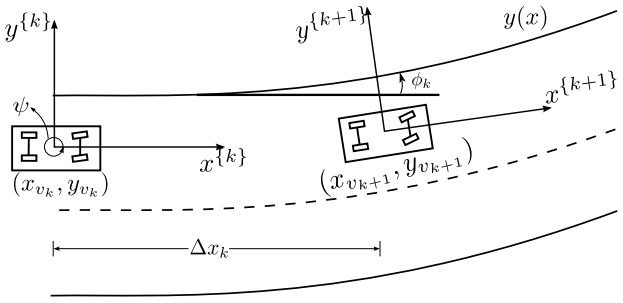

Fig. 3. Road model represented by a Clothoid curve along with vehicle motion representation.

A. Prediction Model

The vehicle model is approximated by the Ackerman bicycle model

$$\begin{bmatrix} \dot{x}_k \\ \dot{y}_k \end{bmatrix} = \begin{bmatrix} \Delta x_k\ cos\ \theta_k \\ \Delta y_k\ sin\ \theta_k \end{bmatrix} \tag{21}$$

Fig. 3 shows the egomotion of the vehicle from the local coordinate frame $(x^{\{k\}}, y^{\{k\}})$ to the frame $(x^{\{k+1\}}, y^{\{k+1\}})$. Considering the longitudinal vehicle motion, Δx, and the Clothoid curve presented in (8), the prediction model can be obtained as follows

$$\mathbf{x}_k = \mathbf{f}_{k-1}(\Delta x_k, \mathbf{x}_{k-1}) + \mathbf{u}_{k-1}(\psi_{k-1}) + \mathbf{v}_k \tag{22}$$

$$\mathbf{f}_{k-1}(\Delta x_k, \mathbf{x}_{k-1}) = \begin{bmatrix} 1 & \Delta x_k & \frac{\Delta x_k{}^2}{2} & \frac{\Delta x_k{}^3}{6} & 0 \\ 0 & 1 & \Delta x_k & \frac{\Delta x_k{}^2}{2} & 0 \\ 0 & 0 & 1 & \Delta x_k & 0 \\ 0 & 0 & 0 & 1 & 0 \\ 0 & 0 & 0 & 0 & 1 \end{bmatrix} \mathbf{x}_{k-1} \tag{23}$$

$$\mathbf{u}_{k-1} = \begin{bmatrix} 0 & -\psi_{k-1} & 0 & 0 & 0 \end{bmatrix}^T \tag{24}$$

The additive noise $\mathbf{v}$ is a zero mean Gaussian noise with covariance $\mathbf{Q}$. The vehicle location as well as the yaw rate ψ are obtained from the vehicle navigation system.

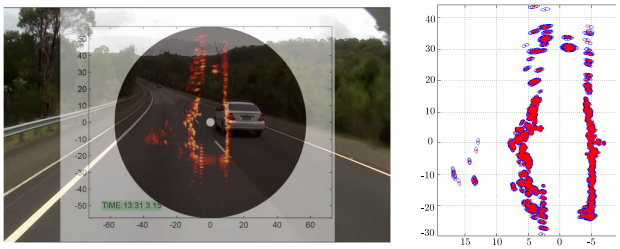

(a) (b)

Fig. 4. (a) Raw radar image superimposed on a colour image of the environment. Brigther pixels represent returns from highly reflective targets. (b) Radar observations modelled as Gaussian distributions. Sigma ellipses error are represented by the blue ellipses around each radar target in red.

B. Observation model used in the Kalman Filter

Fig. 4(a) shows a raw radar image as well as a colour image of the environment acquired on a highway road. The radar sensor position is represented by the white circle at the coordinate $(0,0)$. Fig. 4(b) illustrates how the radar observations are modelled as Gaussian distributions after segmenting the raw radar data. Red points represent the radar measurements and the uncertainty of each radar return is represented by the sigma ellipses error in blue.

As can be seen in Fig. 4(a), there are some radar observations detected not only on the road, but also far from the borders. In order to remove these outlier measurements, we can perform gating and data association, which involves identifying the origin of measurements and associating them to a specific particle or Clothoid curve from which they could have been generated. As stated in [18], the ellipsoidal validation gate is optimal for a linear observation model with additive noise

$$\mathbf{y}_k = \mathbf{H}_k\mathbf{x}_k + \mathbf{w}_k \tag{25}$$

where the additive noise $\mathbf{w}$ is zero-mean Gaussian. The validity of the measurement $\mathbf{z}_k$ is determined from its Mahalanobis distance from the predicted observation $\mathbf{y}_k$ in the y-direction, and so outlier observations are removed and are not considered in the weighting process for that specific particle.

Because several radar returns detected within a region on the edge of the road are correlated, the assumption of treating them as independent measurements is not valid. Rather, each return detects a point on the surface of the roadside bump, and we must devise a model to map this to the clothoid line. Hence, the radar measurements are first clustered into regions of $5m$ long along each side of the road then those Gaussian distributions found within these regions are fused into single Gaussian distribution or pseudo-observation. Clusters represent a simple surface model that maps the shape of the bump onto the clothoid that runs along the centre line of the bump. It is illustrated by the blue ellipses error on each side of the road in Fig. 5(a) for the clothoid curve represented by the blue lines in Fig. 5(b).

The predicted observations in the Kalman filter are represented by a 1-dimensional vector $\mathbf{y}_k$. This vectors is constructed by the y-coordinates of the Clothoid curve which are

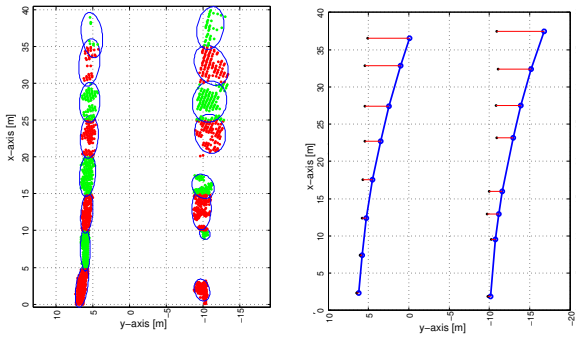

(a) (b)

Fig. 5. (a) Fusion of multiple Gaussian distribution into a single Gaussian functions in blue. (b) Centroids of the combined Gaussian distributions represented by the black dots along with a Clothoid curve in blue.

aligned with the y-coordinate of the centroid of the pseudo-observations belonging to the left and right edges of the road. These centroids are represented by black points in Fig. 5(b). Their locations are defined by its x-and-y coordinates on the road plane, that is, $[(xL_j, yL_j), \ldots, (xL_{ML}, yL_{ML})]^T$, $j = 1 \ldots ML$ and $[(xR_j, yR_j), \ldots, (xR_{MR}, yR_{MR})]^T$, $j = 1 \ldots MR$. Where ML and MR are the number of pseudo-observations on each edge of the road respectively. The error considered here corresponds to the discrepancy in the y-coordinates. The complete predicted measurement vector $\mathbf{y}_k$ is represented by

$$\mathbf{y_k} = [yL_1 \ldots yL_{ML}, yR_1 \ldots yR_{MR}]^T \tag{26}$$

The matrix $\mathbf{H}$ that associates the propagated particle with the predicted observations in (25) is given by

$$\mathbf{H}_k = \begin{bmatrix} 1 & xL_1 & \frac{xL_1^2}{2} & \frac{xL_1^3}{6} & 0 \\ \ldots & \ldots & \ldots & \ldots & \ldots \\ 1 & xL_{M_l} & \frac{xL_{M_l}^2}{2} & \frac{xL_{M_l}^3}{6} & 0 \\ 1 & xR_1 & \frac{xR_1^2}{2} & \frac{xR_1^3}{6} & -1 \\ \ldots & \ldots & \ldots & \ldots & \\ 1 & xR_{M_r} & \frac{xR_{M_r}^2}{2} & \frac{xR_{M_r}^3}{6} & -1 \end{bmatrix} \tag{27}$$

The elements in the last column in $\mathbf{H}_k$, whose value is -1, enable us to obtain the predicted observation on the right edge of the road.

VI. RESULTS

A. Experiment setup and radar specifications

The experiments presented in this work were conducted on a highway road. The driven trajectory comprises about $5km$. Besides the radar scanner and a GPS sensor, a stereo camera was used for display purposes. These sensors were mounted on the test vehicle shown in Fig. 6(a). The radar sensor frame rate was $2Hz$. The vehicle navigation system provided GPS position per second. [1]

[1]See available videos at
www-personal.acfr.usyd.edu.au/ahernandez/roadEstimation.avi

(a) (b)

Fig. 6. (a) Test vehicle used in the experiments. (b) Radar sensor and GPS mounted on the vehicle.

Fig. 7. Radar setup on the test-vehicle.

The specifications for the radar sensor are listed in Table I. Some of these parameters can be associated to the information presented in Fig. 7 which shows the configuration of the radar sensor mounted on the test-vehicle.

TABLE I
RADAR SENSOR SPECIFICATIONS

Field of view	360^o
Maximum detection range R_{max}	60m
Operation frequency	94 GHz
Uncertainty in range σ_r	0.25 cm
Uncertainty in orientation angle σ_θ	1^o
Horizontal beam width γ_h	2^o
Vertical beam width γ_v	8^o
Height of the radar on top of the vehicle H	2.4 m

B. Raw radar image interpretation

The brightness of features in a radar image depends on the fraction of the radiated energy that is returned back to the radar sensor from targets detected in the environment. The intensity of this backscattered energy is basically dependent on the following aspects:

1) Surface roughness of the target.
2) Radar viewing and surface geometry relationship.
3) Moisture content and electrical properties of the target.

The surface of the road is considered as a smooth area if the height fluctuations are much smaller than the radar wavelength, which is about $3mm$ for the MMW radar used in the experiment. A smooth surface causes specular reflections of the incident energy, usually away from the sensor; hence, only a small amount of energy is returned to the radar. Therefore, the surface of the road in Fig. 4(a) appears as darker toned areas. In contrast, when the surface height variations approach the radar wavelength, the surface will appear 'rough', then some reflections will be sent back to the radar receiver. Berms located on the sides of the road will strongly reflect the radar signal intensity back to the radar receiver. In this case, the borders will appear as a brighter tone as shown on the right side of the road in Fig. 4(a).

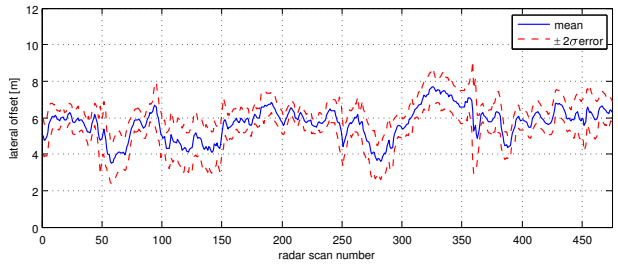

(a) Lateral offset to the left edge of the road along the driven trajectory.

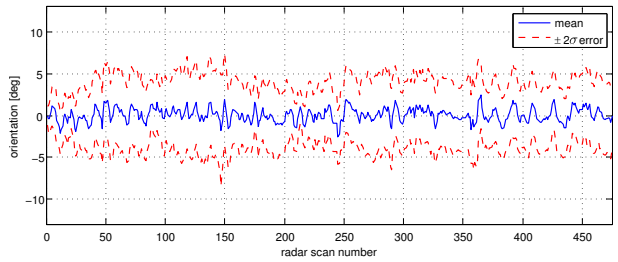

(b) Orientation angle of the road with respect to the radar.

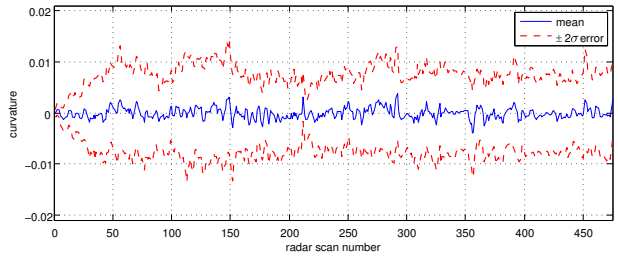

(c) Curvature of the road.

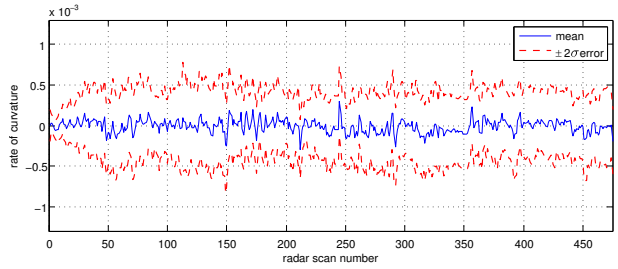

(d) Rate of curvature of the road

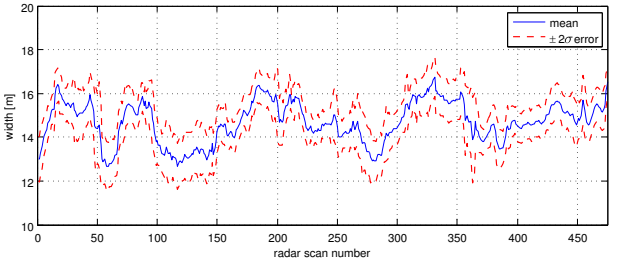

(e) Width of the road

Fig. 8. Estimated parameters that best describe the geometry of the road ahead of the vehicle. The $\pm 2\sigma$ confidence interval is represented by the red lines in each Figure.

The results presented in Fig. 8 depict the estimated parameters that describe the geometry of the road ahead of the vehicle. Each figure shows the estimated mean as well as the $\pm 2\sigma$ uncertainty area. Fig. 8(a) shows the lateral offset that is measured from the radar sensor to the left edge of the road. Variations in the lateral offset are smoother in sections of the road where there is either a berm, a rock wall or a guard rail located on the left edge of the road. The uncertainty in the estimation of this parameter decreases in these sections of the road because the radar targets locations are concentrated within a narrower spatial area as it can be seen from the scans number 10 to 50 in Fig. 8(a). The estimation of the lateral offset for this section of the road correspond to the environment illustrated in Fig. 9(a).

Fig. 8(b) illustrates the orientation of the road with respect to the radar coordinate frame. In this case the confidence interval increases when the vehicle is turning. An example of this issue can be seen from the scans number 100 to 150. Fig. 8(c) and Fig. 8(d) show the curvature and rate of curvature of the road. The values for these estimated parameters are very close to zero because the curves along this particular road are not highly curved. From Fig. 8(c), it is also observed that the confidence interval starts to increase when the vehicle is approaching a curve. An example of this aspect can be also seen from the scans number 100 to 150. Fig. 8(e) shows the width of the road. The actual width of the lane is approximately $8m$. The width of each road shoulder on each side of the road is about $2m$. However, the mean of the estimated parameters fluctuates from $12.5m$ to $16.5m$ because the road estimation was based on targets such as berms, guard rails, rock walls, and trees located on the sides of the road, rather than detecting the marking lanes.

Fig. 9(a) shows some multipath echoes on the left side of the road due to multiple signal reflections from the wall rock to the vehicle. By applying vaildation gate, the proposed algorithm discriminates these multiple signal reflections as they could affect the road estimation process if these returns are detected close to valid targets, such as those belonging to the wall rock.

Fig. 10 illustrates a sequence of four consecutive frames. As can be seen in Fig. 10(h), most of the radar returns on the left side of the road belong to the berm located about $8m$ on the left and trees detected beyond the road boundaries. This as can be seen in the colour image in Fig. 10(g). At this step, the algorithm provides a suitable representation of the road. However, in Fig. 10(f), the estimation of the road is slightly affected by the lack of radar measurements near the left edge of the road. In this case, the algorithm estimates the edges of the road based on observations detected on the right road boundary. As soon as radar targets are detected on

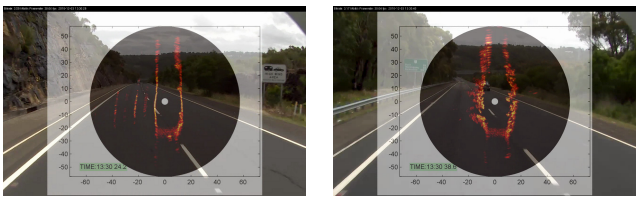

(a) (b)

Fig. 9. (a) Radar measurements obtained when a rock wall is located on the side of the road. (b) Radar measurements that correspond to targets such as trees or vegetation near the edges of the road.

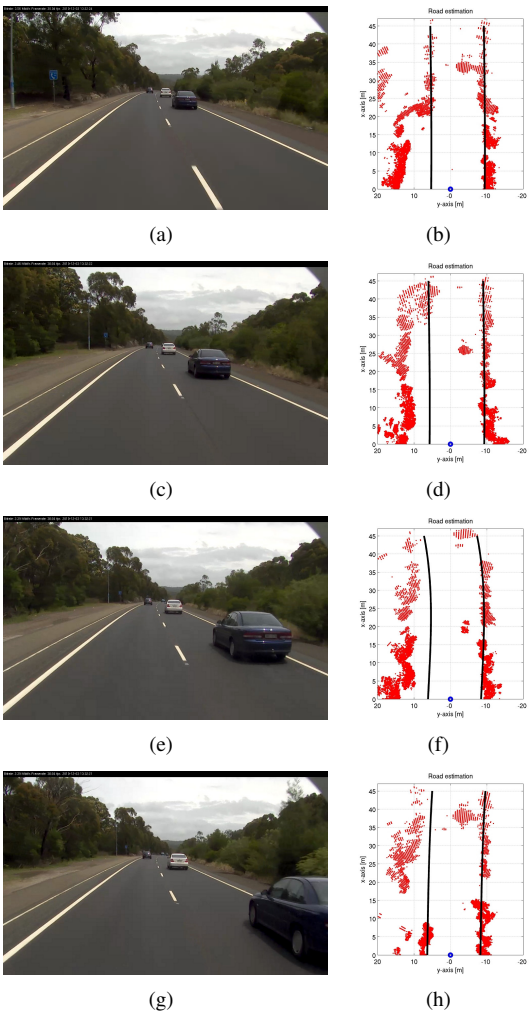

(a) (b) (c) (d) (e) (f) (g) (h)

Fig. 10. Consecutive radar scans than show when the road estimation is slightly affected by the absence of a berm or a wall near on either edge of the road. However, the estimation of the road is corrected as soon as radar returns are detected on the left side again as shown in Fig. (d).

the left side of the road the estimation is corrected as shown in Fig. 10(d) and Fig. 10(b). When the radar sensor does not receive any return from either side of the road, the estimation of the road is based on the prediction model unless no radar information is detected for more than a number of scans. In such a case, the curvature, C_0, and the rate of curvate, C_1, are set to zero and the other parameters are initialised to their previous estimated values.

VII. CONCLUSIONS AND FUTURE WORKS

This paper presented a probabilistic approach for road estimation using a radar sensor. The radar measurements were modelled as Gaussian distributions and integrated to a Kalman particle filter, and it estimated the parameters that best described the geometry of the road using a Clothoid function to model the shape of road boundaries.

Experimental results with data acquired on a highway road validated the proposed approach. The obtained results are encouraging considering that no special work (such as adding infrastructure) was performed on the berms limiting the road. This implies that results could be improved by proper maintenance of the road.

Although the assumption of considering both edges or the road as parallel curves provided encouraging results, in future work, we will propose to estimate the geometry of the road modelling each road boundary independently.

VIII. ACKNOWLEDGEMENTS

We would like to thank to Javier Martinez, Vijay Nichani and David Orchansky from the Australian Centre for Field Robotics for their valuable assistance with the experiments presented in this paper.

This work has been partially supported by CONACYT and SEP Mexico, the Australian Centre for Field Robotics and the New South Wales State Government.

REFERENCES

[1] E. D. Dickmanns and A. Zapp, "A Curvature-Based Scheme for Improving Road Vehicle Guidance by Computer Vision", SPIE, vol. 727, 1986, pp 161-168.

[2] E. D. Dickmanns, B. Mysliwetz and T. Christians, "An Integrated Spatio-Temporal Approach to Automatic Visual Guidance of Autonomous Vehicles", *Transactions on Systems, Man, and Cybernetics*, vol. 20, no. 6, 1990, pp 1273-1284.

[3] E. D. Dickmanns, B. D. Mysliwetz, "Recursive 3-D Road and Relative Ego-State Recognition", *Transactions on Pattern Analysis and Machine Intelligence*, vol. 14, no. 2, 1992, pp 199-213.

[4] K. Kluge, "Extracting road curvature and orientation from image edge points without perceptual grouping into features", *Proceedings of Intelligent Vehicles Symposium*, 1994, pp 109-114.

[5] B. Southall and C. J. Taylor, "Stochastic road shape estimation", *in ICCV Eighth International Conference on Computer Vision*, vol. 1, 2001, pp 205.

[6] M. Isard and A. Blake, "ICondensation: unifying low-level and high-level tracking in a stochastic framework", *in ECCV European Conference of Computer Vision*, 1998.

[7] N. Apostoloff, "Vision based lane tracking using multiple cues and particle filtering", Master's thesis, Australian National University, 2005.

[8] R. Aufrere, R. Chapuis, and F. Chausse, "A fast and robust vision based road following algorithm", *Proceedings of Intelligent Vehicles Symposium*, 2000, pp 192-197.

[9] W. Wijesoda, K. Kodagoda, and A. P. Balasuriya, "Road boundary detection and tracking using ladar", *Transaction on Robotics and Automation*, vol. 20, 2004, pp 456-464.

[10] R. Aufrere, C. Mertz, and C. Thorpe, Multiple sensor fusion for detecting location of curbs, walls, and barriers, *Proceedings of Intelligent Vehicles Symposium*, 2003, pp 126-131.

[11] H. Loose, U. Franke, and C. Stiller, "Kalman Particle Filter for Lane Recognition on Rural Roads", *Proceeding of Intelligent Vehicles Symposium*, vol. 1, 2009, pp 60-65.

[12] M. Tsogas, N. Floudas, P. Lytrivis, A. Amditis, and A. Polychronopoulos, "Combined lane and road attributes extraction by fusing data from digital map, laser scanner and camera", *Informat. Fusion*, 2010.

[13] G. Brooker, R. Hennessey, C. Lobsey, M. Bishop, and E. Widzyk-Capehart, "Seeing through Dust and Water Vapor: Millimetre Wave Radar Sensors for Mining Applications", *Journal of Field Robotics*, vol. 24, no. 7, 2007, pp 527-557.

[14] J. Ryde and N. Hillier, "Performance of Laser and Radar Ranging Devices in Adverse Environmental Conditions", *Journal of Field Robotics*, vol. 26, no. 9, 2009, pp 712-727.

[15] R. Lamm, B. Psarianos, and T. Mailaender, *Highway design and traffic safety engineering handbook*, McGraw-Hill; 1999.

[16] B. Ristic, S. Arulampalam and N. Gordon, *Beyond the Kalman Filter: Particle Filters for Tracking Applications*, Artech House; 2004.

[17] V. S. Zaritskii, V. B. Svetnik, and L. I. Shinelevich, "Monte Carlo Technique in Problems of Optimal Data Processing", *Auto. Remo. Cont.*, vol. 12, 1975, pp 95-103

[18] T. Bailey, B. Upcroft, and H. Durrant-Whyte, *International Conference on Information Fusion*, 2006, pp 1-6.